Eur. Phys. J. Appl. Phys. (2017) 79: 30401
DOI: 10.1051/epjap/2017160406

THE EUROPEAN PHYSICAL JOURNAL APPLIED PHYSICS

Regular Article

Iron oxide nanoparticles stabilized by lignocellulosic waste as green adsorbent for Cr(VI) removal from wastewater

Immaculate L.A. Ouma[a], Eliazer B. Naidoo, and Augustine E. Ofomaja

Biosorption and Wastewater Treatment Research Laboratory, Vaal University of Technology, Private Bag X021, Vanderbijlpark 1900, South Africa

Received: 28 October 2016 / Received in final form: 28 April 2017 / Accepted: 6 July 2017

Abstract. Magnetite nanoparticles and magnetite-pine cone nanocomposite were prepared and applied in the adsorption of hexavalent chromium from water. Pine cone powder stabilized the nanoparticles and acted as a support while simultaneously introducing functional groups which improved metal adsorption. The nanocomposite retained the nanoparticles magnetic properties while improving chromium adsorption efficiency. Adsorption of hexavalent chromium on both materials was pH and concentration dependent with the most efficient adsorption occurring at pH 2 and 75 mg/L. On both materials, chromium adsorption was spontaneous with Gibbs free energy values of −19.2 kJ mol^{-1} to −23.7 kJ mol^{-1} and −18.0 kJ mol^{-1} to −24.2 kJ mol^{-1} for nanoparticles and nanocomposite respectively between 298 K and 319 K. The changes in enthalpy and entropy were determined to be 44.4 kJ mol^{-1}, 212.7 J K^{-1} mol^{-1} and 78.3 kJ mol^{-1}, 323.3 J K^{-1} mol^{-1} for the prepared nanoparticles and nanocomposite respectively.

1 Introduction

Chromium is a highly toxic transition metal which has been reported to be carcinogenic, mutagenic and a strong oxidant [1]. It has several uses in industry which may lead to environmental exposure during disposal. Chromium ions exist in oxidation states ranging from −IV to +VI but the trivalent and the hexavalent state are the most prevalent due to their stability [2]. The trivalent state forms relatively insoluble hydroxides as compared to the hexavalent state and is therefore less available for uptake [3]. It is an essential micronutrient in humans used in combination with various enzymes for fat, protein and sugar transformation [4]. The highly soluble and mobile hexavalent form is the most toxic form of chromium and has attracted a lot of investigations [5,6]. Several remediation techniques including ion exchange, electro-chemical precipitation, electrocoagulation, electrodeposition and adsorption have been applied in its removal from waste water [7–13]. However, most of these methods suffer drawbacks due to the cost of materials, instrumentation, high energy requirements and complexity of their designs. Adsorption is favored because of its simplicity in design, versatility and cost effective operation which is a result of the availability of many low cost adsorbents capable of reducing contaminant concentrations in water [11]. Environmentally friendly materials are continually being investigated for their potential in adsorption. The application of nanotechnology in wastewater treatment has been a topic of interest in the past few years. Nanoparticles are versatile in applications and can be applied in various areas of research including the remediation of heavy metal contaminated waste water. Nanoparticles particularly iron oxide magnetic nanoparticles have certain advantages over conventional adsorbents which include large surface area to volume ratios, high reactivity, ability to be functionalized, low diffusion resistance when applied in a packed column and the ability to be separated from treated water by applying a magnetic field [14]. Nanoparticles have sizes in the nanometre scale and are highly charged leading to agglomeration (size increase) and ultimately loss of desired surface properties. Therefore, to keep them as stable dispersions, avoid agglomeration and loss of surface properties, capping agents need to be added to nanoparticle surfaces [15]. Various capping agents have been applied to stabilize nanoparticles in aqueous solution and these include silica, ligands of nitrogen containing organic chemicals and polyfunctional organic acids. In this work, pine cone powder obtained from biocompatible agricultural waste materials was used to stabilize iron oxide magnetic nanoparticles to form a nanocomposite which was used for adsorption of Cr(VI) from water. The powder was pre-treated with Fenton's reagent to oxidize some of the surface groups and provide more binding sites

[a] e-mail: oumachieng@gmail.com

for iron oxide while also eliminating soluble organic components which may lead to contamination of the treated water [16].

2 Experimental

2.1 Materials

Pine tree cones were collected from Vaal University of Technology in Vanderbijlpark. They were washed and oven dried at 90 °C to remove sand and other impurities. The scales were peeled and crushed then sieved to obtained particles with sizes below 90 μm which were used for further experiments.

Cr(VI) solution for the experiments was prepared by dissolving a known amount of $K_2Cr_2O_7$ in deionized water. Solutions for the experiments were prepared from the stock solution by appropriate dilutions with deionized water.

2.2 Methods

2.2.1 Preparation of Fenton's treated pine cone powder

Fenton's reagent was prepared by measuring 303 cm^3 of 30% H_2O_2 and 6.993 g of $FeSO_4{\cdot}7H_2O$ into separate 1000 cm^3 volumetric flasks. The pH of Fe^{2+} was adjusted to between 3 and 4.5 using 0.1 M H_2SO_4. One hundred grams of pine cone powder was weighed and transferred into a 2000 cm^3 three-necked round bottom flask, fitted with a gas inlet, magnetic stirrer and condenser. The flask and its contents were degassed for 15 min followed by passing nitrogen gas for another 15 min. Then 250 cm^3 of Fe^{2+} solution was added and heated at 50 °C for 30 min. This was followed by the addition of 250 cm^3 of H_2O_2 and heating for a further 30 min. The resulting powder was filtered and washed with deionized water till a clear filtrate was obtained. The washed powder was dried at 80 °C for 8 h.

2.2.2 Synthesis of iron oxide nanoparticles

One hundred millilitres of deionized water was added to a three-necked round bottom flask fitted with a magnetic stirrer and a condenser. The water was degassed for 15 min at 80 °C followed by bubbling nitrogen gas for 15 min to create an inert atmosphere. To the water 3.1 g of $FeCl_3{\cdot}6H_2O$ and 2.1 g $FeSO_4{\cdot}7H_2O$ salts were added with vigorous stirring. NH_4OH was added for co-precipitation and the stirring was continued for a further 45 min. The formed black precipitate was washed with deionized water and ethanol several times each time allowing the precipitate to settle under the influence of a magnet and decanting the supernatant. The washed precipitate was dried in a vacuum oven overnight at 60 °C.

2.2.3 Preparation of pine cone-iron oxide nanocomposite

One hundred millilitres of deionized water was added to a three neck round bottom flask fitted with a magnetic stirrer and a condenser. The water was degassed for 15 min at 80 °C followed by bubbling nitrogen gas for 15 min to create an inert atmosphere. To the water 1.5 g of Fenton's treated pine cone powder, 3.1 g of $FeCl_3{\cdot}6H_2O$ and 2.1 g $FeSO_4{\cdot}7H_2O$ salts were introduced into the flask with vigorous stirring. NH_4OH was added for co-precipitation and the stirring was continued for a further 30 min under inert atmosphere. The formed black precipitate was washed with deionized water and ethanol to remove excess ammonia. The washed precipitate was dried in a vacuum oven overnight at 60 °C.

Scanning electron microscopy (SEM) analysis was carried out on a Carl Zeiss, Sigma scanning electron microscope. X-ray diffraction (XRD) analysis was carried out on a Bruker AXS D8 advanced diffractometer equipped with a Cu $K\alpha$ ($\lambda = 1.5418$ Å) X-ray source.

2.2.4 Adsorption studies

To determine the effect of solution pH, concentration and temperature on chromium adsorption, batch adsorption experiments were carried out. A Cr(VI) stock solution of 1000 mg/L was prepared and diluted to 100 mg/L in separate volumetric flasks and the solution pH in each flask was varied between 2 and 12 using 0.01 M HCl and 0.01 M NaOH to study the effect of pH on adsorption. Then, 0.5 g of each adsorbent was introduced into a sealable flask containing Cr(VI) solution and stirred for 2 h. To study the effect of initial solution concentration, the procedure was repeated with solutions of pH 2 and concentrations ranging from 25 ppm to 200 ppm in separate flasks. The Cr(VI) concentration was determined spectrophotometrically following the diphenylcarbazide method at a wavelength of 540 nm [17]. To determine the effect of temperature the Cr(VI) solutions were heated to the desired temperature before the addition of adsorbent and maintained at the same temperature throughout the experiment.

3 Results and discussion

3.1 Characterization

The prepared nanoparticles and nanocomposite formed dispersions in water (Fig. 1) and upon the introduction of a permanent magnet, they were retained allowing the water to be decanted. Introduction of pine cone to coat the particles did not alter the magnetic properties of the nanoparticles but instead formed a uniform magnetic nanocomposite.

In Figure 2a Fenton's treated pine cone powder is seen to have a smooth porous surface which allows for sequestration of ions [18]. Figure 2b shows that the prepared

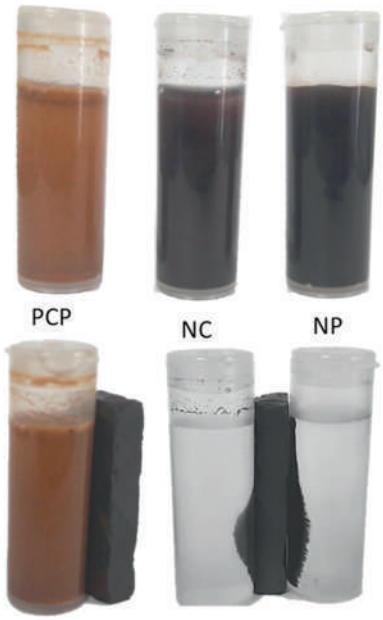

Fig. 1. Pine cone powder (PCP), nanocomposite (NC) and nanoparticles (NP) dispersed in water and magnetic separation of nanocomposite (NC) and nanoparticles (NC).

nanoparticles are agglomerated, possibly due to high surface energies resulting from their small sizes [19]. During the formation of magnetite nanoparticles ferric and ferrous ions are precipitated in the presence of hydroxyl ions to form nanoparticles. The nanoparticle surfaces are therefore covered with excess hydroxyl groups from solution and these group interactions as well as magnetic attraction increase agglomeration [20]. In the presence of pine cone powder, magnetite particles are precipitated within the pores (Fig. 1c) leading to breakage of the pine cone hence exposing more surfaces while simultaneously stabilizing the nanoparticles (Fig. 1d) [21].

The X-ray diffraction pattern of Fenton's treated pine cone in Figure 3 shows three major peaks at 22.3°, 37.82° and 44.06°. These peaks are shifted from previously reported values for crystalline cellulose (I) at 15.3°, 21.3° and 34.0° and amorphous cellulose (II) at 26.1°, 36.2° and 40.1° [22]. Fenton's oxidation generally reduces the amount of cellulose in pine cone therefore may account for the absence of some cellulose peaks in the diffraction pattern [16]. Diffraction pattern of the as-synthesized nanoparticles reveals peaks at 30.75°, 36.09°, 43.81°, 54.03°, 57.67° and 63.26° attributed to crystalline planes with Miller indices (2 2 0), (3 1 1), (4 0 0), (4 2 2), (5 1 1) and (4 4 0) respectively. The pattern matches the standard diffraction pattern for synthetic magnetite (JCPDS card no. 19-0629) confirming the inverse spinel structure of the as-synthesized nanoparticles [23,24]. Diffraction peaks for magnetite and cellulose from pine cone are present in the nanocomposite indicating it consists of both pine cone and magnetite, the peaks corresponding to magnetite are broadened and slightly shifted possibly due to a decrease in crystallinity because of the presence of amorphous cellulose in the nanocomposite. The binding of pine cone on the surface of magnetite nanoparticles may cause strain on bound surface atoms that differs from unbound surface atoms therefore resulting in a shift of the diffraction peaks [22,25,26]. Average particle sizes estimated from Scherrer's equation were found to be 7.19 ± 1.02 nm and 6.95 ± 0.86 nm for the nanoparticles and nanocomposite respectively [27,28]. The smaller nanocomposite sizes as compared to the nanoparticles suggests that the added biomass was bound to nanoparticle surfaces hence hindering further crystal growth and stabilizing the particles [25,26].

3.2 Adsorption studies

3.2.1 Solution pH

Batch adsorption of chromium (VI) ions was carried out on magnetite nanoparticles (NP) and the nanocomposite (NC). In Figure 5 it is observed that nanoparticles had a lower adsorption efficiency than the nanocomposite. Addition of pine cone to the nanoparticles led to improved adsorption of chromium ions due to better separation and stability of particles hence increasing surface areas [29]. The higher adsorption efficiency as shown by the nanocomposite is possibly contributed to by the presence of pine cone power which contains functional groups with the ability to sequester chromium ions [30]. The stability of different hexavalent chromium species in solution is highly dependent on the solution pH as described by Saha and Orvig [2]. The species occur as H_2CrO_4, $HCrO_4^-$, $Cr_2O_7^{2-}$ and CrO_4^{2-} with increasing solution pH from pH $<$ 1, pH 2–6 and pH $>$ 6 respectively [2]. Figure 4 shows that the percentage removal for hexavalent chromium is higher at low solution pH and decreases with increasing solution pH for both adsorbents. At acidic pH there is a high concentration of hydrogen ions in solution which protonate the binding sites allowing the negatively charged Cr(VI) to be attracted and bound on the adsorbent surface [31]. This in turn leads to the removal of hexavalent chromium ions from solution by electrostatic attraction [32]. For this study pH 2 was taken as the optimum pH since at this pH there was the highest adsorption of hexavalent chromium.

3.2.2 Solution concentration

Adsorption of hexavalent chromium on magnetite nanoparticles and magnetite-pine cone nanocomposite was carried out at concentrations between 25 mg/L and 200 mg/L to determine the effect of solution concentration on the sorption process. Figure 5 shows that at lower initial solution concentration, there was higher adsorption efficiency with almost complete chromium removal at 25 mg/L. The higher efficiency at lower solution concentrations was due to availability of adsorption sites with low adsorbate concentration therefore high amounts of chromium were taken up. However, an increase in

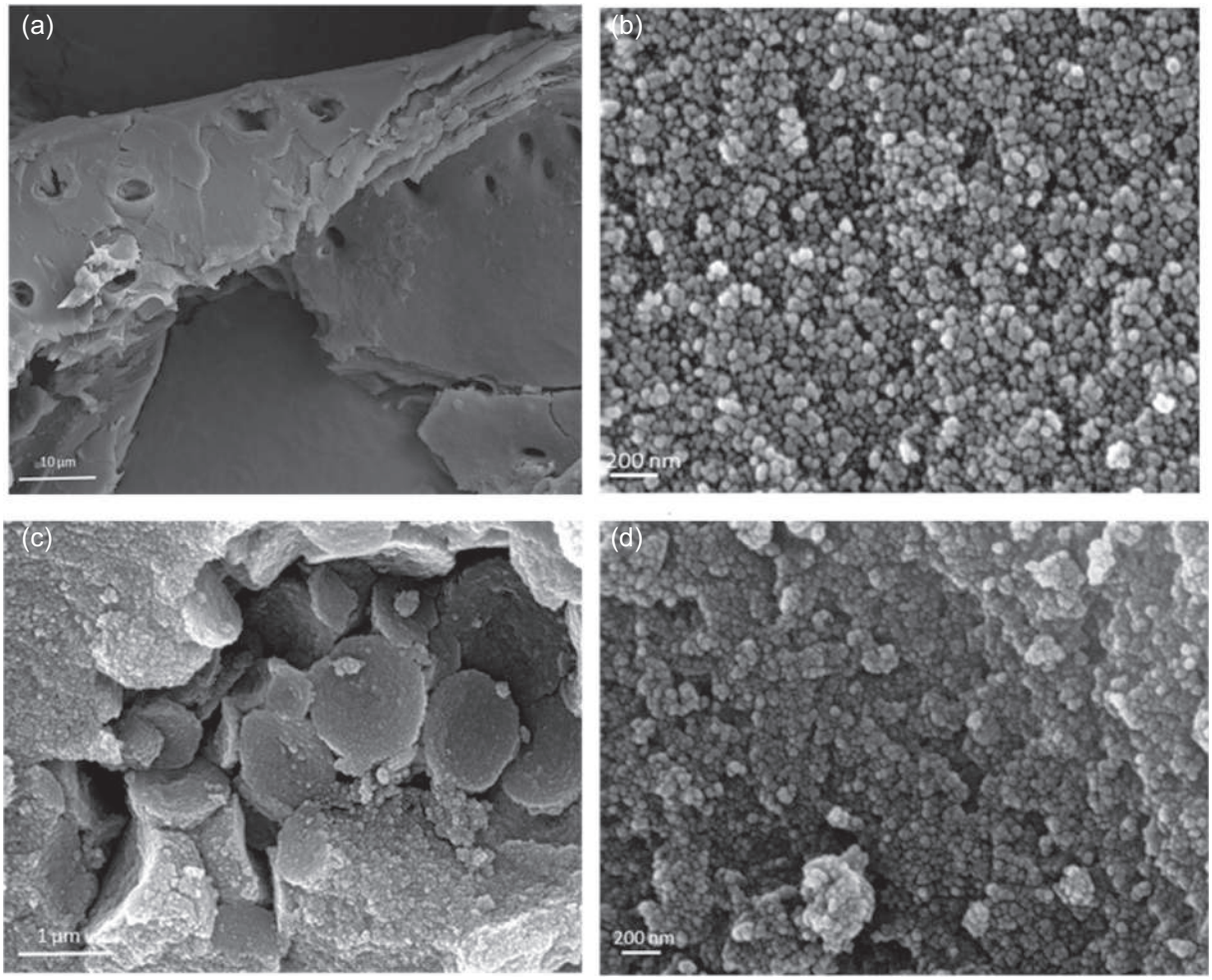

Fig. 2. SEM image of (a) pine cone powder, (b) iron oxide nanoparticles, (c) and (d) pine cone-iron oxide nanocomposites.

chromium/adsorbent ratio led to a decrease in adsorption efficiency while increasing the amount of chromium adsorbed (mg) per adsorbent unit (g). Higher initial solution concentrations provide higher mass transfer of adsorbate from solution to solid phase hence improving the interaction between the adsorbate and adsorbent resulting in increasing adsorption capacity [30,33]. At all solution concentrations, the nanocomposite had a higher adsorption capacity and efficiency than nanoparticles thereby indicating that the introduction of pine cone improved the adsorption properties of iron oxide nanoparticles. The suitable solution concentration for hexavalent chromium adsorption was identified as 75 mg/L where both efficiency and capacity were optimized.

3.3 Adsorption isotherms

The adsorption results were modeled following the Langmuir and Freundlich isotherms to determine the iso therm that better predicts hexavalent chromium adsorption onto magnetite nanoparticles and magnetite-pine cone nanocomposite.

3.3.1 Langmuir isotherm

Langmuir isotherm described by equation (1) assumes that adsorption occurs on a homogenous surface with identical adsorption sites hence monolayer coverage on the adsorbent surface and no further adsorption takes place after the sites are occupied [34].

$$\mathrm{Q_e} = \frac{q_\mathrm{m} K_\mathrm{L} \mathrm{C_e}}{1 + K_\mathrm{L} \mathrm{C_e}}, \tag{1}$$

$$\frac{\mathrm{C_e}}{\mathrm{Q_e}} = \frac{\mathrm{C_e}}{q_\mathrm{m}} + \frac{1}{K_\mathrm{L}}, \tag{2}$$

where $\mathrm{C_e}$ is the solution concentration at equilibrium, $\mathrm{Q_e}$ is the adsorption capacity at equilibrium, q_m is the maximum adsorption capacity and K_L is the Langmuir constant. The linearized form (Eq. (2)) is used to obtain a plot of $\frac{\mathrm{C_e}}{\mathrm{Q_e}}$ against $\mathrm{C_e}$ from which the constants can be determined. Adsorption data for both the nanoparticles and nanocomposite (Tab. 1) fitted the isotherm with correlation coefficients close to unity.

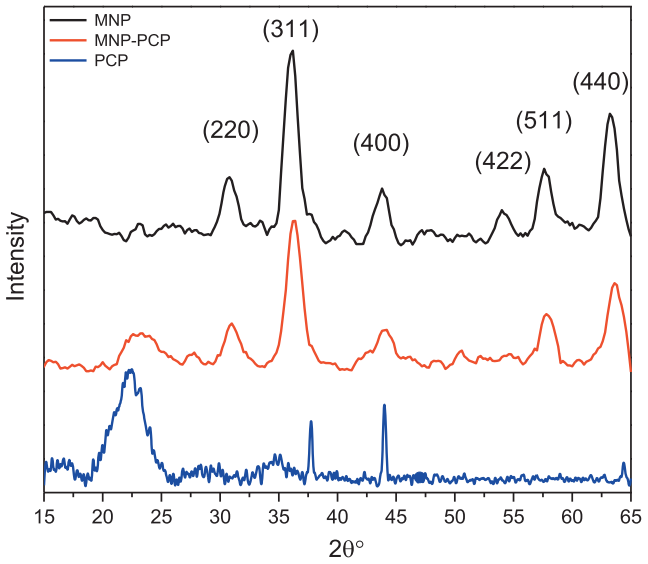

Fig. 3. XRD spectra of pine cone powder (PCP), nanoparticles (NP) and nanocomposite (NC).

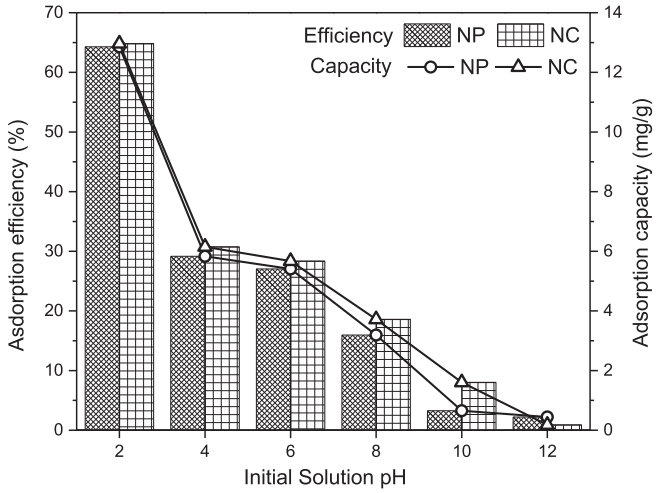

Fig. 4. Adsorption efficiency and capacity of magnetite nanoparticles (NP) and magnetite pine cone nanocomposite (NC) for Cr(VI) species at different solution pH.

3.3.2 Freundlich isotherm

The Freundlich isotherm relates the amount of an adsorbate adsorbed per unit weight of adsorbent to the adsorbate equilibrium concentration. The relation is described by equation (3) below:

$$\mathrm{Q_e} = K_\mathrm{f} \mathrm{C_e}^{1/n}, \tag{3}$$

$$\log \mathrm{Q_e} = \log K_\mathrm{f} + 1/n \log \mathrm{C_e}, \tag{4}$$

where $\mathrm{Q_e}$ is the equilibrium adsorption capacity, $\mathrm{C_e}$ is the concentration of solution at equilibrium and K_f and n the characteristic constants. The data can be fitted in the logarithmic form (Eq. (4)) and used to generate a linear plot of $\log \mathrm{Q_e}$ against $\log \mathrm{C_e}$ from which the constants and correlation coefficient can be determined. The adsorption data was fitted and coefficients determined for the Freundlich isotherm model (Tab. 2). From the model parameters, the data better fitted the Langmuir than Freundlich model hence signifying that the adsorption sites were identical on a homogenous surface.

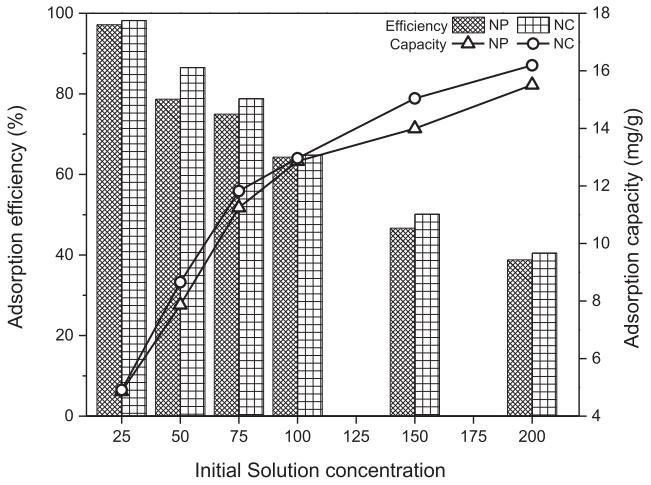

Fig. 5. Effect of initial solution concentration on Cr(VI) removal.

3.3.3 Thermodynamic studies

The adsorption of hexavalent chromium on both adsorbents was repeated at 298, 304, 309, 314 and 319 K to determine the thermodynamic parameters for the adsorption process. The Gibbs free energy ΔG, enthalpy ΔH and entropy ΔS for the adsorption were determined by the relations:

$$\Delta G = -RT \ln K_\mathrm{C}, \tag{5}$$

$$\Delta G = \Delta H - T\Delta S, \tag{6}$$

where ΔG is the change in Gibbs free energy, R is the gas constant (8.314 J mol^{-1} K^{-1}), T is the temperature in Kelvin and K_C is the equilibrium constant [16,35]. Thermodynamic data determined for the adsorption of hexavalent chromium on both adsorbents is presented in Table 3. The greater negative value for Gibbs free energy as temperature increased indicated a spontaneous reaction which increased in spontaneity with an increase in temperature [36–38]. Therefore, the adsorption of chromium onto both magnetite nanoparticles and magnetite-pine cone nanocomposite was more favorable at higher temperatures [39]. Change in enthalpy and entropy were determined from the intercept and slope after plotting ΔG against temperature. A positive value of enthalpy for the adsorption of hexavalent chromium on magnetite nanoparticles and magnetite-pine cone nanocomposite indicated an endothermic process while a positive change in entropy signified increased randomness at the solid-solution interface during Cr(VI) adsorption on both magnetite nanoparticles and magnetite-pine cone nanocomposite.

Table 1. Langmuir isotherm fitting data for chromium adsorption on iron oxide nanoparticles and iron oxide pine cone powder nanocomposite.

	Nanoparticles			Nanocomposite		
Temperature (K)	q_m (mg g^{-1})	K_L (dm^3 mg^{-1})	r^2	q_m (mg g^{-1})	K_L (dm^3 mg^{-1})	r^2
298	13.514	0.045	0.997	13.643	0.054	0.996
304	14.347	0.065	0.992	14.556	0.088	0.991
309	14.925	0.071	0.996	15.949	0.154	0.996
314	17.065	0.110	0.992	17.182	0.219	0.996
319	17.637	0.148	0.994	18.416	0.238	0.992

Table 2. Freundlich isotherm fitting data for chromium adsorption on iron oxide nanoparticles and iron oxide pine cone powder nanocomposite.

	Nanoparticles			Nanocomposite		
Temperature (K)	n (dm^3 g^{-1})	K_f	r^2	n (dm^3 g^{-1})	K_f	r^2
298	2.372	0.608	0.938	2.472	0.529	0.893
304	2.999	0.365	0.958	3.383	0.290	0.961
309	3.002	0.344	0.974	3.968	0.202	0.960
314	3.584	0.223	0.985	5.189	0.144	0.965
319	3.839	0.190	0.979	5.280	0.132	0.973

Table 3. Thermodynamic parameters for Cr(VI) adsorption by magnetite nanoparticles and magnetite-pine cone nanocomposite.

	Nanoparticles			Nanocomposite		
	ΔG	ΔH	ΔS	ΔG	ΔH	ΔS
Temperature (K)	(kJ mol^{-1})	(kJ mol^{-1})	(J K^{-1} mol^{-1})	(kJ mol^{-1})	(kJ mol^{-1})	(J K^{-1} mol^{-1})
298	−19.202	44.352	212.74	−18.032	78.2814	323.25
304	−20.553			−19.142		
309	−20.639			−22.709		
314	−22.589			−23.602		
319	−23.731			−24.205		

4 Conclusion

Iron oxide nanoparticles and a nanocomposite consisting of iron oxide nanoparticles and pine cone powder were synthesized. Characterization of the prepared nanoparticles and nanocomposite revealed the synthesized nanoparticles diffraction pattern matched the diffraction pattern of synthetic magnetite and that the addition of pine cone stabilized their surfaces resulting in reduced agglomeration and smaller particles. The synthesized materials were applied in the adsorption of hexavalent chromium from water and incorporation of pine cone significantly improved the adsorption of Cr(VI). Hexavalent chromium adsorption on the prepared nanoparticles and nanocomposite was highest at acidic pH and low initial solution concentrations and decreased with an increase in solution pH and concentration. Equilibrium studies showed that the adsorption data was better modelled by Langmuir isotherm indicating monolayer coverage of the adsorbent surface. Thermodynamic parameters for hexavalent chromium adsorption on both adsorbents revealed that the adsorption was spontaneous at all temperatures, was endothermic in nature and had increased randomness at the solution-solid interface.

Authors would like to thank the South African National Research Foundation and Vaal University of Technology for sponsoring this research.

References

1. T. Burks, A. Uheida, M. Saleemi, M. Eita, M.S. Toprak, M. Muhammed, Sep. Sci. Technol. **48**, 1243 (2013)
2. B. Saha, C. Orvig, Coord. Chem. Rev. **254**, 2959 (2010)
3. P. Wu, S. Li, L. Ju, N. Zhu, J. Wu, P. Li, Z. Dang, J. Hazard. Mater. **219**, 283 (2012)
4. V. Gómez, M.P. Callao, Trends Anal. Chem. **25**, 1006 (2006)
5. R.F.F. Yu, F.H.H. Chi, W.P.P. Cheng, J.C.C. Chang, Chem. Eng. J. **255**, 568 (2014)
6. M.Y. Arica, G. Bayramoğlu, Colloids Surf. A: Physicochem. Eng. Aspects **253**, 203 (2005)
7. N. Kongsricharoern, C. Polprasert, Water Sci. Technol. **34**, 109 (1996)
8. S. Rengaraj, K.H. Yeon, S.H. Moon, J. Hazard. Mater. **87**, 273 (2001)
9. K. Dermentzis, A. Christoforidis, E. Valsamidou, A. Lazaridou, N. Kokkinos, Global Nest. J **13**, 412 (2011)
10. S. Survilienė, O. Nivinskienė, A. Češunienė, A. Selskis, J. Appl. Electrochem. **36**, 649 (2006)

11. R. Elangovan, L. Philip, K. Chandraraj, Chem. Eng. J. **141**, 99 (2008)
12. R. Say, E. Birlik, Z. Erdemgil, A. Denizli, A. Ersöz, J. Hazard. Mater. **150**, 560 (2008)
13. J.O. Babalola, T.M. Bamidele, E.A. Adeniji, N.W. Odozi, A.M. Olatunde, M.O. Omorogie, Model. Earth Syst. Environ. **2**, 190 (2016)
14. X. Peng, F. Xu, W. Zhang, J. Wang, C. Zeng, M. Niu, E. Chmielewská, Colloids Surf. A: Physicochem. Eng. Aspects **443**, 27 (2014)
15. E. Cheraghipour, A.M. Tamaddon, S. Javadpour, I.J. Bruce, J. Magn. Magn. Mater. **328**, 91 (2013)
16. M.E. Argun, S. Dursun, M. Karatas, M. Gürü, Bioresour. Technol. **99**, 8691 (2008)
17. M.E. Bishop, P. Glasser, H. Dong, B. Arey, L. Kovarik, Geochim. Cosmochim. Acta **133**, 186 (2014)
18. F. Deniz, Environ. Prog. Sustain. Energy **34**, 1267 (2015)
19. M. Hua, S. Zhang, B. Pan, W. Zhang, L. Lv, Q. Zhang, J. Hazard. Mater. **211**, 317 (2012)
20. A.A. Alqadami, M. Naushad, M.A. Abdalla, T. Ahamad, Z.A. Alothman, S.M. Alshehri, RSC Adv. **6**, 22679 (2016)
21. P. Panneerselvam, N. Morad, K.A. Tan, J. Hazard. Mater. **186**, 160 (2011)
22. A.E. Ofomaja, E.B. Naidoo, Chem. Eng. J. **175**, 260 (2011)
23. S. Rajput, C.U. Pittman, D. Mohan, J. Colloid Interface Sci. **468**, 334 (2016)
24. K. Tao, H. Dou, K. Sun, Colloids Surf. A: Physicochem. Eng. Aspects **320**, 115 (2008)
25. A.E. Pirbazari, E. Saberikhah, S.S.S. Habibzadeh Kozani, Water Resour. Ind. **7**, 23 (2014)
26. W.S. Li, Z.X. Shen, H.Y. Li, D.Z. Shen, X.W. Fan, J. Raman Spectrosc. **32**, 862 (2001)
27. D.K. Kim, Y. Zhang, W. Voit, K.V. Rao, M. Muhammed, J. Magn. Magn. Mater. **225**, 30 (2001)
28. G. Gnanaprakash, S. Mahadevan, T. Jayakumar, P. Kalyanasundaram, J. Philip, B. Raj, Mater. Chem. Phys. **103**, 168 (2007)
29. L. Feng, M. Cao, X. Ma, Y. Zhu, C. Hu, J. Hazard. Mater. **217**, 439 (2012)
30. H. Ucun, Y.K. Bayhan, Y. Kaya, A. Cakici, O. Faruk Algur, Bioresour. Technol. **85**, 155 (2002)
31. N.A. Fathy, S.T. El-Wakeel, R.R. Abd El-Latif, J. Environ. Chem. Eng. **3**, 1137 (2015)
32. P. Miretzky, A.F. Cirelli, J. Hazard. Mater. **180**, 1 (2010)
33. S. Dawood. T.K. Sen, Water Res. **46**, 1933 (2012)
34. A.O. Dada, A.P. Olalekan, A.M. Olatunya, O. Dada, IOSR J. Appl. Chem. **3**, 38 (2012)
35. M.O. Omorogie, J.O. Babalola, E.I. Unuabonah, J.R. Gong, Clean Technol. Environ. Policy **18**, 171 (2016)
36. Y. Cantu, A. Remes, A. Reyna, D. Martinez, J. Villarreal, H. Ramos, S. Trevino, C. Tamez, A. Martinez, T. Eubanks, J.G. Parsons, Chem. Eng. J. **254**, 374 (2014)
37. M. Xu, H. Wang, D. Lei, D. Qu, Y. Zhai, Y. Wang, J. Environ. Sci. **25**, 479 (2013)
38. J.O. Babalola, B.A. Koiki, Y. Eniayewu, A. Salimonu, J.O. Olowoyo, V.O. Oninla, H.A. Alabi, A.E. Ofomaja, M.O. Omorogie, J. Environ. Chem. Eng. **4**, 3527 (2016)
39. U. Kumar, Int. J. Environ. Sci. Dev. **2**, 334 (2011)